Segmentation of Ischemic Stroke Lesions in Multi-spectral MR Images Using Weighting Suppressed FCM and Three Phase Level Set

Chaolu Feng[1,2(✉)], Dazhe Zhao[1,2], and Min Huang[1,3]

[1] School of Computer Science and Engineering, Northeastern University, Shenyang 110819, Liaoning, China
[2] Key Laboratory of Medical Image Computing of Ministry of Education, Northeastern University, Shenyang 110819, Liaoning, China
fengchl@ise.neu.edu.cn
[3] State Key Laboratory of Synthetical Automation for Process Industries, Northeastern University, Shenyang 110819, Liaoning, China

Abstract. Accurate segmentation of ischemic lesions is still a challenging task. In this paper, we propose a framework to extract ischemic lesions from multi-spectral MR images. In the proposed framework, MR images of each modality are first segmented into brain tissues and ischemic lesions by weighting suppressed fuzzy c-means. Preliminary lesion segmentation results are then fused among all the imaging modalities by majority voting. The fused segmentation results are finally refined by a three phase level set method. The level set formulation is defined on multi-spectral images with the capability of dealing with intensity inhomogeneities. The proposed framework has been applied to the MICCAI 2015 ISLES challenge. According to the ranking rules of the challenge, the proposed framework took the second place and the fourth place in sub-acute lesion segmentation and acute stroke estimation, respectively.

Keywords: Lesion segmentation · Fuzzy c-means · Label fusion · Level set

1 Introduction

Ischemic stroke generally manifests as a loss of neurological brain function due to the sudden loss of blood circulation to an area of the brain [15]. It is by far the most common type of stroke and has become to be the most frequent cause of permanent disability in adults worldwide and the third leading cause of death in industrialized countries [17]. Magnetic resonance imaging (MRI) has become the modality of choice for diagnosing and evaluating ischemic stroke in clinic due to its excellent soft tissue contrast and multi-spectral imaging capability [11]. As ischemic stroke lesions usually change over time and remote and secondary changes may also occur in response to the injury, it is therefore necessary to characterize the injury and changes with different acquisition parameters and distinctive spectral signatures [4].

A. Crimi et al. (Eds.): BrainLes 2015, LNCS 9556, pp. 233–245, 2016.
DOI: 10.1007/978-3-319-30858-6_20

In clinical practice, diffusion weighted imaging (DWI), T1-weighted (T1w) and T2-weighted (T2w) images, and fluid attenuated inversion recovery (FLAIR) images are often used to diagnose ischemic stroke, locate the lesions and monitor their progression [15]. In the acute phase of stroke, DWI is particularly sensitive to detect the anatomical location and infarcted territory of the lesions and reveal differentiation of brain tissues with hyperintense signal [5]. The lesions appear slightly to strongly hyperintense in T2w and FLAIR images for stroke in sub-acute stage, whereas they are decreasingly hyperintense in DWI images and hypointense in T1w images [13]. For chronic ischemic stroke, lesions appear as hyperintense in FLAIR images with some heterogeneity within the lesion due to ongoing gliosis and demyelination [14]. In contrast, intensities of ischemic lesions are hypointense in T1w images for stroke in the more chronic phase [9]. Figure 1 shows an example of intensity characteristics of ischemic stroke lesions that are in the sub-acute phase.

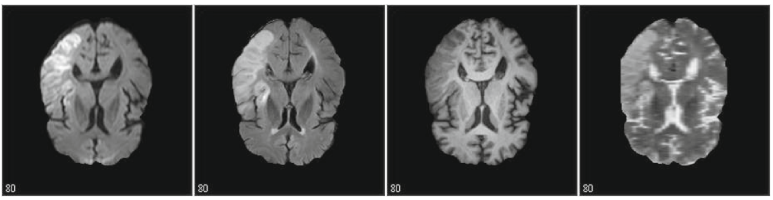

(a) DWI (b) FLAIR (c) T1w (d) T2w

Fig. 1. Intensity characteristics of ischemic stroke lesion in different imaging modalities. Images come from http://www.isles-challenge.org/.

Above all, early diagnosis of ischemic lesions in multi-spectral magnetic resonance images is particularly important for ischemic stroke prevention and treatment [13]. But it is really challenging for neuro-radiologists to read the images slice-by-slice [18]. Although lesion segmentation is able to rescue radiologists from the labor of image reading, manual segmentation is tedious, time consuming, and prone to intraobserver and interobserver variability [11]. Therefore, a few semi-automatic or automatic segmentation methods have been proposed in the literature [6,7,11,16]. However, due to varieties of possible shapes and locations of ischemic lesions, and noise and intensity inhomogeneity in MR images, segmentation of ischemic lesions is still a challenging task [8].

In this paper, we propose a framework to automatically segment ischemic stroke lesions in multi-spectral images (e.g. DWI, T1w, T2w, and FLAIR). The rest of this paper is organized as follows. The proposed framework is described in Sect. 2. Experimental results and quantitative evaluation are given in Sect. 3. This paper is finally summarized and discussed in Sect. 4.

2 Method

In this paper, we suppose that the input images of different modalities have already been rigidly registered in the same coordinate system and non-brain tissues have already been removed from the images. Lesion segmentation is then performed by the proposed framework which consists of three major steps: (1) preliminary segmentation, (2) segmentation fusion, and (3) boundary refinement. More details will be given in the following subsections.

2.1 Preliminary Segmentation of Lesions and Normal Tissues

Given an image I_i from the i-th imaging modality, the image characterizes an intrinsic physical property of human brain, which ideally takes a specific intensity for each type of brain tissue (white matter (WM), gray matter (GM), and cerebrospinal fluid (CSF)) and lesion. That is to say, the image I_i approximately takes distinct constant values c_{i1}, c_{i2}, ..., and c_{iN} for $N-1$ brain tissues and the lesions in disjoint regions Ω_1, Ω_2, ..., and Ω_N, i.e.

$$I_i(\mathbf{x}) \approx c_{ij} \quad \text{for} \quad \mathbf{x} \in \Omega_{\mathrm{j}}. \tag{1}$$

where $j = 1, 2, ..., N$. Note that the variable i takes all integers in the interval of $[1, L]$ where L is the total number of imaging modalities. It is obvious that intensities in the set $I_{ij} = \{I_i(\mathbf{x}) : \mathbf{x} \in \Omega_j\}$ form a cluster with the cluster centroid $m_{ij} \approx c_{ij}$. This clustering property indicates that intensities in the image domain Ω can be classified into N clusters.

To classify these intensities, we define

$$\mathcal{F}_i = \int_{\Omega} \sum_{j=1}^{N} \lambda_{ij} \parallel I_i(\mathbf{x}) - c_{ij} \parallel^2 u_{ij}^q(\mathbf{x}) d\mathbf{x} \tag{2}$$

where $\parallel * \parallel$ is the Euclidean distance between measured intensity $I_i(\mathbf{x})$ and the cluster centroid c_{ij}, q is any real number that is not less than 1, λ_{i1}, λ_{i2}, ..., λ_{iN} are positive weighting coefficients for the N clusters, and $u_{ij}(\mathbf{x})$ is the membership function that indicates whether voxel $\mathbf{x}$ belongs to the j-th tissue. In fact, the smaller parameter λ_{ij} is, the greater the j-cluster is, and vice versa.

It is obvious that the proposed method, which we call *weighting suppressed fuzzy c-means*, is a generalization of the standard fuzzy c-means. Note that the objective function defined above is the same with standard fuzzy c-means if λ_{i1}, λ_{i2}, ..., λ_{iN} are all set to be 1. This objective function is minimized when high membership values are assigned to voxels, intensities of which are close to the centroid, and low membership values are assigned to the voxels if they are far from the centroids under the condition $\sum_{j=1}^{N} u_{ij}(\mathbf{x}) = 1$ where $u_{ij}(\mathbf{x}) \in [0, 1]$. For convenience, we represent the constants c_{i1}, c_{i2}, ..., and c_{iN} with a vector $\mathbf{c}_i = (c_{i1}, c_{i2}, ..., c_{iN})$, the member functions u_{i1}, u_{i2}, ..., and u_{iN} with a vector $\mathbf{u}_i = (u_{i1}, u_{i2}, ..., u_{iN})$. Thus, the vectors $\mathbf{c}_i$ and $\mathbf{u}_i$ are the variables of the energy function $\mathcal{F}_i$, which can therefore be written as $\mathcal{F}_i(\mathbf{c}_i, \mathbf{u}_i)$.

Energy minimization of $\mathcal{F}_i(\mathbf{c}_i, \mathbf{u}_i)$ can be achieved by alternately minimizing it with respect to each of its variables $\mathbf{c}_i$ and $\mathbf{u}_i$. For fixed $\mathbf{u}_i$, we minimize $\mathcal{F}_i(\mathbf{c}_i, \mathbf{u}_i)$ with respect to $\mathbf{c}_i$ by resolving $\frac{\partial \mathcal{F}_i(\mathbf{c}_i, \mathbf{u}_i)}{\partial \mathbf{c}_i} = \mathbf{0}$ where $\mathbf{0}$ is the constant vector with value 0. It is obvious that $\mathcal{F}_i(\mathbf{c}_i, \mathbf{u}_i)$ is minimized at $\hat{\mathbf{c}}_i = (\hat{c}_{i1}, \hat{c}_{i2}, ..., \hat{c}_{iN})$, given by

$$\hat{c}_{ij} = \frac{\int_\Omega I_i(\mathbf{x}) u_{ij}^q(\mathbf{x})}{\int_\Omega u_{ij}^q(\mathbf{x})} \tag{3}$$

where $j = 1, 2, ..., N$.

For the case $q > 1$, it can be shown that $\mathcal{F}_i(\mathbf{c}_i, \mathbf{u}_i)$ is minimized at $\hat{\mathbf{u}}_i(\mathbf{x}) = (\hat{u}_{i1}(\mathbf{x}), \hat{u}_{i2}(\mathbf{x}), ..., \hat{u}_{iN}(\mathbf{x}))$ for fixed $\mathbf{c}_i$, given by

$$\hat{u}_{ij}(\mathbf{x}) = \frac{\left(\lambda_{ij} \| \ I_i(\mathbf{x}) - c_{ij} \ \|^2\right)^{\frac{1}{1-q}}}{\sum_{k=1}^{N} \left(\lambda_{ik} \ \| \ I_i(\mathbf{x}) - c_{ik} \ \|^2\right)^{\frac{1}{1-q}}} \tag{4}$$

where $j = 1, 2, ..., N$.

For the case $q = 1$, it can be shown that the minimizer $\hat{\mathbf{u}}_i(\mathbf{x}) = (\hat{u}_{i1}(\mathbf{x}), \hat{u}_{i2}(\mathbf{x}), ..., \hat{u}_{iN}(\mathbf{x}))$ is given by

$$\hat{u}_{ij}(\mathbf{x}) = \begin{cases} 1, & j = j_{min}(\mathbf{x}) \\ 0, & j \neq j_{min}(\mathbf{x}) \end{cases} \qquad j = 1, 2, ..., N \tag{5}$$

where

$$j_{min}(\mathbf{x}) = \underset{j}{argmin} \left(\lambda_{ij} \ \| \ I_i(\mathbf{x}) - c_{ij} \|^2\right). \tag{6}$$

In fact, segmentation of WM, GM, CSF, and stroke lesions in this step is performed in an iterative process, which will be described in detail in Sect. 2.4.

2.2 Fusion of Preliminary Segmentation Results of Lesions

Label fusion is one of the most important steps for multi-spectral segmentation due to its significance in merging useful knowledge of different labels [3]. In the literature, many efforts have already been devoted to developing effective and accurate label fusion strategies [2,3,12]. As one of the well known label fusion strategies, majority voting is much more straightforward and concise [1]. Therefore, majority voting is used in the proposed framework to fuse segmentation results of ischemic stroke lesions obtained by the above described fuzzy c-means method. The judge rule is that candidate voxels are regarded as lesions only if (1) they are considered as brain lesions in FLAIR images, and (2) they are viewed as brain lesions in more than 1 imaging modality beside FLAIR.

2.3 Boundary Refinement of Brain Lesions Using 3-Phase Level Set

Since miss- and over- segmentations may arise in the above mentioned two steps. A three phase level set method is proposed in this subsection as the third step to

refine segmentation boundaries of the lesions. The proposed method can be seen as an extension of the local intensity clustering (LIC) model with the capability of segmenting ischemic stroke lesions from multi-spectral MR images [10].

Before defining the energy formulation of the proposed level set method, we first view inhomogeneous intensities of an observed MR brain image I_i coming from the i-th imaging modality, which is defined on a continuous domain $\Omega \subset R^3$, as a product of the true image J_i and the bias field b_i, i.e.,

$$I_i(\mathbf{x}) = b_i(\mathbf{x})J_i(\mathbf{x}) + n_i(\mathbf{x}) \tag{7}$$

where $\mathbf{x} \in \Omega$ and n_i is the zero-mean additive noise.

Consider a relatively small spherical neighborhood with a radius ρ centered at a given point $\mathbf{y} \in \Omega$, defined by $\mathcal{O}_\mathbf{y} \triangleq \{\mathbf{x} :| \mathbf{x} - \mathbf{y} |\leq \rho\}$. The bias field b_i in the neighborhood can be ignored due to its slowly and smoothly varying property. Taking into account the constant intensity c_{ij} of the true image J_i in Ω_j as mentioned in Sect. 2.1, we obtain

$$b_i(\mathbf{x})J_i(\mathbf{x}) \approx b_i(\mathbf{y})c_{ij} \quad \text{for} \quad \mathbf{x} \in \Omega_\mathrm{j} \cap \mathcal{O}_\mathbf{y}. \tag{8}$$

This local intensity clustering property allows us to apply the standard K-means algorithm in the following continuous form to classify these local inhomogeneous intensities in the neighborhood $\mathcal{O}_\mathbf{y}$. Taking all images of the L imaging modalities into account, we define

$$\mathcal{E}_y = \sum_{j=1}^{N} \gamma_j \int_{O_y} \left(\sum_{i=1}^{L} \chi_i \parallel I_i(\mathbf{x}) - b_i(\mathbf{y})c_{ij} \parallel^2 \right) u_j(\mathbf{x}) d\mathbf{x} \tag{9}$$

where γ_j is a weighting coefficient used to control size of the j-th tissue, χ_i is a weighting coefficient for images from the i-th imaging modality, and u_j is the binary membership function of Ω_j. On account of the inherent property of the membership function u_j in representing Ω_j, $\mathcal{E}_\mathbf{y}$ can be rewritten as

$$\mathcal{E}_\mathbf{y} = \sum_{j=1}^{N} \gamma_j \int_{\Omega_j} K_\sigma(\mathbf{x} - \mathbf{y}) \left(\sum_{i=1}^{L} \chi_i \parallel I_i(\mathbf{x}) - b_i(\mathbf{y})c_{ij} \parallel^2 \right) d\mathbf{x} \tag{10}$$

where K_σ is a nonnegative kernel function with the property $\int_{|\mathbf{u}|\leq\rho} K_\rho(\mathbf{u}) = 1$ and $K_\rho(\mathbf{u}) = 0$ for $\mathbf{u} \notin \mathcal{O}_y$.

To ensure the partition $\{\Omega_j\}_{j=1}^N$ of the entire domain Ω to be the one such that $\mathcal{E}_\mathbf{y}$ is minimized for all $\mathbf{y}$ in Ω, we minimize the integral of $\mathcal{E}_\mathbf{y}$ with respect to $\mathbf{y}$ over the entire image domain Ω and define

$$\mathcal{E} = \int_\Omega \left(\sum_{j=1}^{N} \gamma_j \int_{\Omega_j} K_\sigma(\mathbf{x} - \mathbf{y}) \left(\sum_{i=1}^{L} \chi_i \parallel I_i(\mathbf{x}) - b_i(\mathbf{y})c_{ij} \parallel^2 \right) d\mathbf{x} \right) d\mathbf{y}. \tag{11}$$

As our goal is to segment brain lesions, we consider the lesions as one region, brain tissues (WM, GM, and CSF) as the second region, and the background as

the third region. Let H be the Heaviside function and ϕ_1 and ϕ_2 be two level set functions both defined on Ω. We therefore use $M_1(\phi_1, \phi_2) = (1-H(\phi_1))(1-H(\phi_2))$, $M_2(\phi_1, \phi_2) = H(\phi_1)(1-H(\phi_2))$, and $M_3(\phi_1, \phi_2) = H(\phi_2)$ to represent these three regions, respectively, and rewrite $\mathcal{E}$ as

$$\mathcal{E} = \int_{\Omega} \left(\sum_{j=1}^{N} \gamma_j e_j(\mathbf{x}) M_j(\phi_1(\mathbf{x}), \phi_2(\mathbf{x})) \right) d\mathbf{x} \tag{12}$$

where

$$e_j(\mathbf{x}) = \int_{\Omega} K_\sigma(\mathbf{x}-\mathbf{y}) \left(\sum_{i=1}^{L} \chi_i \parallel I_i(\mathbf{x}) - b_i(\mathbf{y}) c_{ij} \parallel^2 \right) d\mathbf{y} \tag{13}$$

For convenience, we represent the bias field b_1, b_2, ..., b_L with a vector $\mathbf{b} = (b_1, b_2, ..., b_L)$ and further rewrite $\mathbf{c}_1$, $\mathbf{c}_2$, ..., and $\mathbf{c}_L$ into a new vector $\mathbf{c} = (\mathbf{c}_1, \mathbf{c}_2, ..., \mathbf{c}_L)$. Thus, the level set functions ϕ_1 and ϕ_2 and the vectors $\mathbf{b}$ and $\mathbf{c}$ are variables of the energy $\mathcal{E}$, which can therefore be written as $\mathcal{E}(\phi_1, \phi_2, \mathbf{b}, \mathbf{c})$.

The energy $\mathcal{E}(\phi_1, \phi_2, \mathbf{b}, \mathbf{c})$ defined above is used as the data term of the final energy functional of the proposed level set formulation, defined by

$$\mathcal{F}(\phi_1, \phi_2, \mathbf{b}, \mathbf{c}) = \mathcal{E}(\phi_1, \phi_2, \mathbf{b}, \mathbf{c}) + \mathcal{P}(\phi_1, \phi_2) + \mathcal{L}(\phi_1, \phi_2). \tag{14}$$

where $\mathcal{P}(\phi_1, \phi_2)$ and $\mathcal{L}(\phi_1, \phi_2)$ are the regularization term and arc length term. These two terms are introduced to maintain the regularity of the level set functions and smooth the 0-level set contours of the level set functions, defined by

$$\mathcal{P}(\phi_1, \phi_2) = \mu_1 \int \frac{1}{2}(\mid \nabla\phi_1(\mathbf{x}) \mid -1)^2 d\mathbf{x} + \mu_2 \int \frac{1}{2}(\mid \nabla\phi_2(\mathbf{x}) \mid -1)^2 d\mathbf{x} \tag{15}$$

and

$$\mathcal{L}(\phi_1, \phi_2) = \nu_1 \int \mid \nabla H(\phi_1(\mathbf{x})) \mid d\mathbf{x} + \nu_2 \int \mid \nabla H(\phi_2(\mathbf{x})) \mid d\mathbf{x} \tag{16}$$

where μ_1, μ_2, ν_1 and ν_2 are weighting coefficients.

Energy minimization of $\mathcal{F}(\phi_1, \phi_2, \mathbf{b}, \mathbf{c})$ can be achieved by alternately minimizing it with respect to each of its variables. For fixed $\mathbf{b}$ and $\mathbf{c}$, we minimize the final energy functional $\mathcal{F}$ using standard gradient descent method and obtain

$$\begin{aligned} \frac{\partial \phi_1}{\partial t} &= \delta(\phi_1)(1-H(\phi_2))(\lambda_1 e_1 - \lambda_2 e_2) \\ &\quad + \mu_1 \left(\nabla^2 \phi_1 - \mathrm{div}\left(\frac{\nabla \phi_1}{\mid \nabla \phi_1 \mid} \right) \right) + \nu_1 \delta(\phi_1) \mathrm{div}\left(\frac{\nabla \phi_1}{\mid \nabla \phi_1 \mid} \right) \end{aligned} \tag{17}$$

and

$$\begin{aligned} \frac{\partial \phi_2}{\partial t} &= \delta(\phi_2)(\lambda_1 e_1 (1-H(\phi_1)) + \lambda_2 e_2 H(\phi_1) - \lambda_3 e_3) \\ &\quad + \mu_2 \left(\nabla^2 \phi_2 - \mathrm{div}\left(\frac{\nabla \phi_2}{\mid \nabla \phi_2 \mid} \right) \right) + \nu_2 \delta(\phi_2) \mathrm{div}\left(\frac{\nabla \phi_2}{\mid \nabla \phi_2 \mid} \right). \end{aligned} \tag{18}$$

For fixed ϕ_1, ϕ_2, and $\mathbf{b}$, the optimal $\tilde{\mathbf{c}} = (\tilde{\mathbf{c}}_1, \tilde{\mathbf{c}}_2, ..., \tilde{\mathbf{c}}_L)$ where $\tilde{\mathbf{c}}_i = (\tilde{c}_{i1}, \tilde{c}_{i2}, ..., \tilde{c}_{iN})$ and $i = 1, 2, ..., L$ minimizes the final energy functional $\mathcal{F}(\phi_1, \phi_2, \mathbf{b}, \mathbf{c})$, given by

$$c_{ij} = \frac{\int I_i(\mathbf{x}) M_j(\phi_1(\mathbf{x}), \phi_2(\mathbf{x}))(b_i * K_\sigma)(\mathbf{x}) d\mathbf{x}}{\int M_j(\phi_1(\mathbf{x}), \phi_2(\mathbf{x}))(b_i^2 * K_\sigma)(\mathbf{x}) d\mathbf{x}}, \; j = 1, 2, ..., N. \tag{19}$$

For fixed ϕ_1, ϕ_2, and $\mathbf{c}$, the optimal $\tilde{\mathbf{b}} = (\tilde{b}_1, \tilde{b}_2, ..., \tilde{b}_L)$ that minimizes the final energy functional $\mathcal{F}(\phi_1, \phi_2, \mathbf{b}, \mathbf{c})$ is given by

$$\tilde{b}_i = \frac{\left(I_i \sum_{j=1}^{N} c_{ij} M_j(\phi_1, \phi_2)\right) * K_\sigma}{\sum_{j=1}^{N} c_{ij}^2 M_j(\phi) * K_\sigma}, \quad i = 1, 2, ..., L. \tag{20}$$

2.4 Implementation

In the implementation of the proposed framework, the choice of K is important but flexible as long as it is a normalized even function and satisfies the property that $K(\mathbf{u}) \geq K(\mathbf{v})$, if $\mid \mathbf{u} \mid < \mid \mathbf{v} \mid$, and $\lim_{|\mathbf{u}| \to \infty} K(\mathbf{u}) = 0$. In this paper, an averaging filter with size of ρ is chosen as K. In our numerical implementation, the stepped Heaviside function H is approximated by a smoothed Heaviside function H_ϵ with $\epsilon = 1$, defined by $H_\epsilon(x) = \frac{1}{2}\left[1 + \frac{2}{\pi} \arctan\left(\frac{x}{\epsilon}\right)\right]$. The derivative of H_ϵ is used to approximate the Dirac delta function δ, which can be written as $\delta_\epsilon(x) = H'_\epsilon(x) = \frac{1}{\pi} \frac{\epsilon}{\epsilon^2 + x^2}$.

The implementation of the proposed framework can be straightforwardly expressed in the following steps.

- Step 1. Segment images of each modality separately using the weighting suppressed fuzzy c-means as described in Sect. 2.1. Update each variable of the energy function defined in Eq. (2) iteratively until the iteration number exceeds a predetermined maximum number or convergence criterion has been reached.
- Step 2. Fuse segmentation results of different modalities using the voting strategy as described in Sect. 2.2.
- Step 3. Refine fused segmentation results using the three phase level set method as described in Sect. 2.3 where the level set functions ϕ_1 and ϕ_2 are initialized to the results of Step 2. Update each variables of energy functional defined in Eq. (14) iteratively until the solution is stable or the iteration number exceeds a predetermined maximum number.

3 Results

To evaluate the proposed framework, we participated in the ischemic stroke lesion segmentation (ISLES) challenge of MICCAI 2015 and applied it to images of the challenge. Figure 2 shows a segmentation example of the proposed framework.

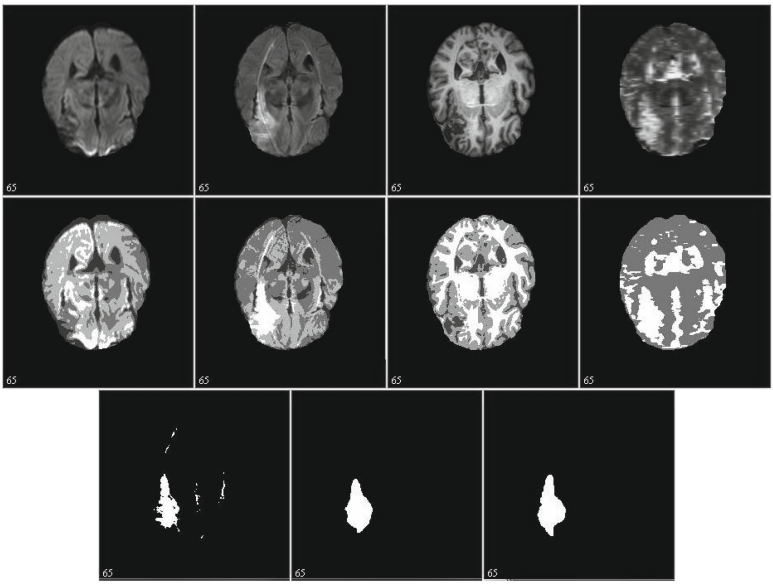

Fig. 2. Segmentation results of the proposed framework on images from four different imaging modalities (http://www.isles-challenge.org/). Orignal images and corresponding preliminary segmentations are given in the 1st and 2nd rows. Fusion result, final segmentation, and the ground truth are given from left to right in the 3rd row.

3.1 Dataset and Parameter Set

The ISLES challenge consists of two sub-challenges: sub-acute ischemic stroke lesion segmentation (SISS) and acute stroke outcome/penumbra estimation (SPES). Dataset of the former includes 28 training cases and 36 testing cases, whereas there are 30 training and 20 testing cases in the latter one. The images are all from MRI and modalities DWI, T1w, T2w, and FLAIR are adopted by the first sub-challenge SISS. In contrast, T1c, T2, DWI, CBF, CBV, TTP, Tmax images are provided by the second sub-challenge SPES. The images are all skull-stripped and have been re-sampled to an isotropic spacing of 1^3 mm (SISS) and 2^3 mm (SPES) and have also been co-registered to the FLAIR (SISS) and T1w contrast (SPES) sequences, respectively.

For SISS, the number of imaging modalities L are set to be 4 with DWI, T1w, T2w, and FLAIR as viewed as the 1st, 2nd, 3rd, and 4th imaging modalities, respectively. When the images are segmented by the proposed weighting suppressed fuzzy c-means separately, we set $N = 4, 3, 2, 4$, respectively. For each imaging modality, e.g., the i-th modality, elements of the cluster centroid vector $\mathbf{c}_i$ are initialized with equally spaced intensities. The other weighting coefficients of the proposed weighting suppressed fuzzy c-means are set to $\lambda_{11} = \lambda_{12} = \lambda_{13} = \lambda_{14} = 1.0$, $\lambda_{21} = 1.0, \lambda_{22} = 0.4, \lambda_{23} = 1.5$, $\lambda_{31} = 1.0, \lambda_{32} = 0.5$, and $\lambda_{41} = \lambda_{42} = \lambda_{43} = \lambda_{44} = 1.0$. The level set function in the third step was

initialized as a binary step function, defined by $\phi(\mathbf{x}) = -c$ for $\mathbf{x}$ inside the initial zero-level contour of ϕ and $\phi(\mathbf{x}) = c$ otherwise. Unless otherwise specified, we set $c = 10$, $\gamma_1 = ... = \gamma_L = 1.0$, $\chi_1 = ... = \chi_L = 1.0$, $\mu_1 = ... = \mu_L = 1.0$, $\nu_1 = ... = \nu_L = 0.1 \times 255 \times 255$, $\Delta t = 0.1$, and $\rho = 6$ in this paper. Note that these parameters can be set to be values learning from training sets.

We have also applied the proposed framework to sub-challenge SPES. We set $N = 3, 5, 3$ for preliminarily segmenting images of modalities CBF, TTP, Tmax, respectively. All weighting coefficients of the proposed weighting suppressed fuzzy c-means are set to be 1.0. As the ground truth provided by the organizers are not smooth enough and there are holes in the lesion-like regions, fusion results obtained by the proposed framework are considered as final segmentation results.

3.2 Evaluation Measures

To evaluate segmentation accuracy of automatic methods that participated in the challenge quantitatively, segmentation results are compared with the reference ground-truth in terms of Dice's coefficient (DC), average symmetric surface distance (ASSD), and Hausdorff distance (HD).

It is well known that the DC is defined as twice of the quotient between intersection size of a pairwise variable and sum of their sizes where the variables are a segmentation result B and the ground truth A for image segmentation, which can therefore be written as

$$DC = \frac{2 \mid A \cap B \mid}{\mid A \mid + \mid B \mid} \tag{21}$$

where $\cap$ is the intersection operator. It is obvious that values of DC are in the interval of $[0, 1]$ with a higher value indicating a better match between A and B.

Considering two sets of surface points that constitute the segmentation result B and the ground truth A, the average surface distance (ASD) is given by

$$ASD(A, B) = \frac{\sum_{a \in A} min_{b \in B}\, d(a, b)}{\mid A \mid} \tag{22}$$

where $d(a, b)$ is the Euclidean distance between the points of a and b. Since $ASD(A, B) \neq ASD(B, A)$, the ASSD can be then defined by

$$ASD(A, B) = \frac{ASD(A, B) + ASD(B, A)}{2}. \tag{23}$$

Note that that ASSD is given in mm, a lower value indicating a better match between the ground truth A and the segmentation result B.

The HD denotes the maximum distance between the obtained volume surface points B and corresponding points in the ground truth A. It can be defined by

$$HD(A, B) = max\{\underset{a \in A}{max}(\underset{b \in B}{min}\, d((a, b))), \underset{b \in B}{max}(\underset{a \in A}{min}\, d((b, a)))\}. \tag{24}$$

Thus, HD is given in mm and a smaller HD value indicates a better agreement of the segmentation result with the ground truth.

3.3 Quantitative Evaluation of the Proposed Framework

As shown in Table 1, 16 teams from all over the world participated in the challenge, where our team information are emphasized in bold font.

Quantitative comparison of the proposed framework with the other participants' methods on images from sub-challenges SISS and SPES are given in Tables 2 and 3, respectively. It is obvious that the proposed framework is the

Table 1. Participants of the ISLES challenge of MICCAI 2015.

Team name	Team leader	Affiliation
UK-Imp1	Chen, Liang	Biomedical Image Analysis Group, Imperial College London
CA-USher	Dutil, Francis	Université de Sherbrooke, Sherbrooke
CN-Neu	**Feng, Chaolu**	**College of Inform. Science and Engineering, Northeastern University, Shenyang**
DE-Dkfz	Goetz, Michael	Junior Group Medical Image Computing, German Cancer Research Center (DKFZ), Heidelberg
BE-Kul1	Haeck, Tom	ESAT/PSI, Department of Electrical Engineering, KU Leuven
FI-Hus	Halme, Hanna	HUS Medical Imaging Center, University of Helsinki and Helsinki University Hospital
CA-McGill	Jesson, Andrew	Centre for Intelligent Machines, McGill University
UK-Imp2	Kamnitsas, Konstantinos	Biomedical Image Analysis Group, Imperial College London
SE-Cth	Mahmood, Qaiser	Signals and Systems, Chalmers University of Technology, Gothenburg
DE-UzL	Maier, Oskar	Institute of Medical Informatics, Universität zu Lübeck
US-Jhu	Muschelli, John	Johns Hopkins Bloomberg School of Public Health
US-Odu	Reza, Syed	Vision Lab, Old Dominion University, Norfolk
BE-Kul2	Robben, David	ESAT/PSI, Department of Electrical Engineering, KU Leuven
TW-Ntust	Wang, Ching-Wei	Graduate Institute of Biomedical Engineering, National Taiwan University of Science and Technology
DE-Ukf	Kellner, Elias	Department of Radiology, Medical Physics, University Medical Center Freiburg
CH-Insel	McKinley, Richard	Department of Diagnostic and Interventional Neuroradiology, Inselspital, Bern University Hospital

Table 2. Accuracy comparison of segmentation results of the proposed framework with the other participants' methods on images from sub-challenge SISS.

Place	Rank	Team	Cases	ASSD	DC	HD
1st	3.25	UK-Imp2 (Kamnitsas, Konstantinos)	34/36	5.96 ± 9.38	0.59 ± 0.31	37.88 ± 30.06
2nd	**3.82**	**CN-Neu (Feng, Chaolu)**	**32/36**	$\mathbf{3.27 \pm 3.62}$	$\mathbf{0.55 \pm 0.30}$	$\mathbf{19.78 \pm 15.65}$
3rd	5.63	FI-Hus (Halme, Hanna)	31/36	8.05 ± 9.57	0.47 ± 0.32	40.23 ± 33.17
4th	6.40	US-Odu (Reza, Syed)	33/36	$6.24 \pm .21$	0.43 ± 0.27	41.76 ± 25.11
5th	6.67	BE-Kul2 (Robben, David)	33/36	11.27 ± 10.17	0.43 ± 0.30	60.79 ± 31.14
6th	6.70	DE-UzL (Maier, Oskar)	31/36	10.21 ± 9.44	0.42 ± 0.33	49.17 ± 29.6
7th	7.07	US-Jhu (Muschelli, John)	33/36	11.54 ± 11.14	0.42 ± 0.32	62.43 ± 28.64
8th	7.54	UK-Imp1 (Chen, Liang)	34/36	11.71 ± 10.12	0.44 ± 0.30	70.61 ± 24.59
9th	7.66	CA-USher (Dutil, Francis)	27/36	9.25 ± 9.79	0.35 ± 0.32	44.91 ± 32.53
10th	7.92	BE-Kul1 (Haeck, Tom)	30/36	12.24 ± 13.49	0.37 ± 0.33	58.65 ± 29.99
11th	7.97	CA-McGill (Jesson, Andrew)	31/36	11.04 ± 13.68	0.32 ± 0.26	40.42 ± 26.98
12th	9.18	SE-Cth (Mahmood, Qaiser)	30/36	10.00 ± 6.61	0.38 ± 0.28	72.16 ± 17.32
13th	9.21	DE-Dkfz (Goetz, Michael)	35/36	14.20 ± 10.41	0.33 ± 0.28	77.95 ± 22.13
14th	10.99	TW-Ntust (Wang, Ching-Wei)	15/36	7.59 ± 6.24	0.16 ± 0.26	38.54 ± 20.36

Table 3. Accuracy comparison of segmentation results of the proposed framework with the other participants' methods on images from sub-challenge SPES.

Place	Rank	Team	Cases	ASSD	DC
1st	2.02	CH-Insel (McKinley, Richard)	20/20	1.65 ± 1.40	0.82 ± 0.08
2nd	2.20	DE-UzL (Maier, Oskar)	20/20	1.36 ± 0.74	0.81 ± 0.09
3rd	3.92	BE-Kul2 (Robben, David)	20/20	2.77 ± 3.27	0.78 ± 0.09
4th	**4.05**	**CN-Neu (Feng, Chaolu)**	**20/20**	$\mathbf{2.29 \pm 1.76}$	$\mathbf{0.76 \pm 0.09}$
5th	4.60	DE-Ukf (Keller, Elias)	20/20	2.44 ± 1.93	0.73 ± 0.13
6th	5.15	BE-Kul1 (Haeck, Tom)	20/20	4.00 ± 3.39	0.67 ± 0.24
7th	6.05	CA-USher (Dutil, Francis)	20/20	5.53 ± 7.59	0.54 ± 0.26

best in terms of ASSD and HD and the second best in DC for sub-challenge SISS. According to the ranking rules of the challenge, which can be found on the website http://www.isles-challenge.org/, the proposed framework finally took the second and fourth places for SISS and SPES, respectively.

4 Conclusion and Discussions

An ischemic lesion segmentation framework has been proposed, which consists of preliminary segmentation, label fusion, and boundary refinement. As most of level set methods are usually time consuming and sensitive to initialization, an improved fuzzy c-means method is first used to coarsely extract ischemic lesions from normal brain tissues. The preliminary segmentation results are only used as initialization of the level set method. Therefore, there is no need to introduce bias correction rules in the first step in consideration of saving time. Quantitative evaluation and comparison with methods that participated in the ISLES challenge have demonstrated advantages of the proposed framework in terms of accuracy.

Note that as the zero level contour of ϕ_2 is used to represent boundaries between brain tissues and the background, update of ϕ_2 is not important for seeking lesion boundaries. Therefore, ϕ_2 can be fixed in the evolution of ϕ_1 to improve computational efficiency. In addition, narrow band implementation can be used to further improve time performance of the proposed level set method.

In the future, we will further improve and validate the proposed method on more datasets, such as MICCAI 2008 lesion segmentation data.

Acknowledgement. This work was supported by the Fundamental Research Funds for the Central Universities of China under grant N140403006, N140402003, and N140407001, the Postdoctoral Scientific Research Funds of Northeastern University under grant No. 20150310, the National Science Foundation for Distinguished Young Scholars of China under Grant Nos. 71325002 and 61225012, the Chinese National Natural Science Foundation under grant Nos. 61172002 and 71071028, the National Key

Technology Research and Development Program of the Ministry of Science and Technology of China under grant 2014BAI17B01, and the Fundamental Research Funds for State Key Laboratory of Synthetical Automation for Process Industries under Grant No. 2013ZCX11.

References

1. Artaechevarria, X., Munoz-Barrutia, A., Ortiz-de Solórzano, C.: Combination strategies in multi-atlas image segmentation: application to brain MR data. IEEE Trans. Med. Imaging **28**(8), 1266–1277 (2009)
2. Asman, A.J., Landman, B.A.: Non-local statistical label fusion for multi-atlas segmentation. Med. Image Anal. **17**(2), 194–208 (2013)
3. Chakravarty, M.M., Steadman, P., Eede, M.C., Calcott, R.D., Gu, V., Shaw, P., Raznahan, A., Collins, D.L., Lerch, J.P.: Performing label-fusion-based segmentation using multiple automatically generated templates. Hum. Brain Mapp. **34**(10), 2635–2654 (2013)
4. Chyzhyk, D., Dacosta-Aguayo, R., Mataró, M., Graña, M.: An active learning approach for stroke lesion segmentation on multimodal MRI data. Neurocomputing **150**, 26–36 (2015)
5. DeIpolyi, A.R., Wu, O., Macklin, E.A., Schaefer, P.W., Schwamm, L.H., Gilberto Gonzalez, R., Copen, W.A.: Reliability of cerebral blood volume maps as a substitute for diffusion-weighted imaging in acute ischemic stroke. J. Magn. Reson. Imaging **36**(5), 1083–1087 (2012)
6. Feng, C., Li, C., Zhao, D., Davatzikos, C., Litt, H.: Segmentation of the left ventricle using distance regularized two-layer level set approach. In: Mori, K., Sakuma, I., Sato, Y., Barillot, C., Navab, N. (eds.) MICCAI 2013, Part I. LNCS, vol. 8149, pp. 477–484. Springer, Heidelberg (2013)
7. Feng, C., Zhao, D., Huang, M.: Image segmentation using CUDA accelerated non-local means denoising and bias correction embedded fuzzy c-means (BCEFCM). Signal Process. **122**, 164–189 (2015). http://dx.doi.org/10.1016/j.sigpro.2015.12.007
8. de Haan, B., Clas, P., Juenger, H., Wilke, M., Karnath, H.O.: Fast semi-automated lesion demarcation in stroke. NeuroImage Clin. **9**, 69–74 (2015)
9. Lee, W.J., Choi, H.S., Jang, J., Sung, J., Kim, T.W., Koo, J., Shin, Y.S., Jung, S.L., Ahn, K.J., Kim, B.S.: Non-stenotic intracranial arteries have atherosclerotic changes in acute ischemic stroke patients: a 3T MRI study. Neuroradiology **57**, 1007–1013 (2015)
10. Li, C., Huang, R., Ding, Z., Gatenby, J.C., Metaxas, D.N., Gore, J.C.: A level set method for image segmentation in the presence of intensity inhomogeneities with application to MRI. IEEE Trans. Image Process. **20**(7), 2007–2016 (2011)
11. Lladó, X., Oliver, A., Cabezas, M., Freixenet, J., Vilanova, J.C., Quiles, A., Valls, L., Ramió-Torrentà, L., Rovira, À.: Segmentation of multiple sclerosis lesions in brain MRI: a review of automated approaches. Inf. Sci. **186**(1), 164–185 (2012)
12. Magon, S., Chakravarty, M.M., Amann, M., Weier, K., Naegelin, Y., Andelova, M., Radue, E.W., Stippich, C., Lerch, J.P., Kappos, L., et al.: Label-fusion-segmentation and deformation-based shape analysis of deep gray matter in multiple sclerosis: the impact of thalamic subnuclei on disability. Hum. Brain Mapp. **35**(8), 4193–4203 (2014)

13. Maier, O., Wilms, M., von der Gablentz, J., Krämer, U.M., Münte, T.F., Handels, H.: Extra tree forests for sub-acute ischemic stroke lesion segmentation in MR sequences. J. Neurosci. Methods **240**, 89–100 (2015)
14. Mitra, J., et al.: Classification forests and markov random field to segment chronic ischemic infarcts from multimodal MRI. In: Shen, L., Liu, T., Yap, P.-T., Huang, H., Shen, D., Westin, C.-F. (eds.) MBIA 2013. LNCS, vol. 8159, pp. 107–118. Springer, Heidelberg (2013)
15. Mitra, J., Bourgeat, P., Fripp, J., Ghose, S., Rose, S., Salvado, O., Connelly, A., Campbell, B., Palmer, S., Sharma, G., et al.: Lesion segmentation from multimodal MRI using random forest following ischemic stroke. NeuroImage **98**, 324–335 (2014)
16. Mortazavi, D., Kouzani, A.Z., Soltanian-Zadeh, H.: Segmentation of multiple sclerosis lesions in MR images: a review. Neuroradiology **54**(4), 299–320 (2012)
17. Rekik, I., Allassonnière, S., Carpenter, T.K., Wardlaw, J.M.: Medical image analysis methods in MR/CT-imaged acute-subacute ischemic stroke lesion: segmentation, prediction and insights into dynamic evolution simulation models. A critical appraisal. Neuroimage Clin. **1**(1), 164–178 (2012)
18. Sridharan, R., et al.: Quantification and analysis of large multimodal clinical image studies: application to stroke. In: Shen, L., Liu, T., Yap, P.-T., Huang, H., Shen, D., Westin, C.-F. (eds.) MBIA 2013. LNCS, vol. 8159, pp. 18–30. Springer, Heidelberg (2013)